polymers

MDPI

Article

Adsorption of Cu(II) by Poly-γ-glutamate/Apatite Nanoparticles

Kuo-Yu Chen * and Wei-Yu Zeng

Department of Chemical and Materials Engineering, National Yunlin University of Science and Technology, Yunlin 64002, Taiwan; jackprotein@hotmail.com

* Correspondence: chenkuo@yuntech.edu.tw; Tel.: +886-5-534-2601 (ext. 4614); Fax: +886-5-531-2071

Abstract: Poly-γ-glutamate/apatite (PGA-AP) nanoparticles were prepared by chemical coprecipitation method in the presence of various concentrations of poly-γ-glutamate (γ-PGA). Powder X-ray diffraction pattern and energy-dispersive spectroscopy revealed that the main crystal phase of PGA-AP was hydroxyapatite. The immobilization of γ-PGA on PGA-AP was confirmed by Fourier transform infrared spectroscopy and the relative amount of γ-PGA incorporation into PGA-AP was determined by thermal gravimetric analysis. Dynamic light scattering measurements indicated that the particle size of PGA-AP nanoparticles increased remarkably with the decrease of γ-PGA content. The adsorption of aqueous Cu(II) onto the PGA-AP nanoparticles was investigated in batch experiments with varying contact time, solution pH and temperature. Results illustrated that the adsorption of Cu(II) was very rapid during the initial adsorption period. The adsorption capacity of PGA-AP nanoparticles for Cu(II) was increased with the increase in the γ-PGA content, solution pH and temperature. At a pH of 6 and 60 °C, a higher equilibrium adsorption capacity of about 74.80 mg/g was obtained. The kinetic studies indicated that Cu(II) adsorption onto PGA-AP nanoparticles obeyed well the pseudo-second order model. The Langmuir isotherm model was fitted well to the adsorption equilibrium data. The results indicated that the adsorption behavior of PGA-AP nanoparticles for Cu(II) was mainly a monolayer chemical adsorption process. The maximum adsorption capacity of PGA-AP nanoparticles was estimated to be 78.99 mg/g.

Keywords: poly-γ-glutamate; apatite; nanoparticles; adsorption; copper ions

Citation: Chen, K.-Y.; Zeng, W.-Y. Adsorption of Cu(II) by Poly-γ-glutamate/Apatite Nanoparticles. *Polymers* **2021**, *13*, 962. https://doi.org/10.3390/polym13060962

Academic Editor: Ángel V. Delgado

Received: 25 February 2021
Accepted: 19 March 2021
Published: 21 March 2021

1. Introduction

Heavy metal water pollution is a severe environmental issue in the developed and developing countries. Copper, one of the main heavy metal pollutants in the water, is produced from different industries like electroplating, mining, copper wire mills, coal, tanning, refining, etc. High concentration of copper is toxic to human and animals due to its high redox activity [1]. It can damage the proteins, DNA, and lipids in the cells [2]. Therefore, it is critical to explore effective and safe approaches to remove copper from polluted water.

Adsorption technique is frequently applied for removing the heavy metal pollutants from contaminated water because of its simple operation, relatively low cost, and high removal efficiency [3]. Various adsorbents are available to the removal of copper ions in wastewater, such as zeolites, clays, fly ash, apatite, activated carbons, chitosan, sodium alginate, cellulose, agricultural wastes, etc. [4]. Apatite is a calcium phosphate mineral with composition and structure similar to those of the mineral phase of natural bones and teeth. There are many types of apatite including hydroxyapatite, fluoroapatite, chloroapatite, and carbonated apatite [5]. Apatite has been utilized in wastewater treatment owing to its low water solubility, good adsorption characteristics, stable in reducing and oxidizing environments, easy preparation, facile modification, environmental-friendly, and low secondary pollution. Therefore, several studies have used apatites to remove aqueous

heavy metals via ion exchange, surface complexation and dissolution/precipitation [6,7]. Nanoparticles have been studied extensively for heavy metal removal due to their high specific surface area and excellent adsorption ability [8]. There are many methods to synthesize apatite nanoparticles, such as chemical precipitation, hydrothermal treatment, emulsion method, sol-gel technique, electrodeposition, and plasma spraying process [9].

Enhanced removal of heavy metal ions through surface modification of apatite particles with carboxylic groups have been shown previously [10–12]. Moreover, it could increase the stability of particles in the aqueous solution. Poly-γ-glutamate (γ-PGA), a natural and biodegradable anionic polypeptide, is produced from various microorganisms such as *Bacillus subtilis* [13]. It has been widely used in medicine, cosmetics, food, agriculture, and water treatment [14]. Previous studies reported that the carboxyl and amide groups of γ-PGA can complex with various metal ions, including Cu(II), Pb(II), Hg(II), Ni(II), Mn(II), Cd(II), Fe(III), Al(III), Cr(III), and U(VI) [15–17]. Some researchers have synthesized apatite by wet chemical method in the presence of amino acid and polypeptide, including aspartic acid, glutamic acid poly-L-aspartate, and γ-PGA, to introduce carboxylic groups onto the apatite surface [12,18–20].

No investigation has been performed on Cu(II) adsorption using γ-PGA/apatite composite nanoparticles. In this study, biocompatible and environmental-friendly apatite nanoparticles were synthesized by coprecipitation method in the presence of γ-PGA to remove Cu(II) species from aqueous solution. The physical and chemical properties of the synthesized poly-γ-glutamate/apatite (denoted as PGA-AP) nanoparticles were characterized through Fourier transform infrared spectroscopy (FTIR), thermal gravimetric analysis (TGA), powder X-ray diffraction (XRD), energy-dispersive spectrometer (EDS) and dynamic light scattering (DLS). This influences of the contact time, solution pH and temperature on Cu(II) removal from aqueous solution by PGA-AP nanoparticles were studied in batch experiments. The adsorption kinetics was investigated with pseudo-first-order and pseudo-second-order models. The adsorption equilibrium was further evaluated by Langmuir and Freundlich isotherms.

2. Materials and Methods

2.1. Materials

γ-PGA with a molecular weight of about 1.2 MDa was provided by Vedan Enterprise Corporation (Taichung, Taiwan). Calcium nitrate tetrahydrate and copper nitrate trihydrate were purchased from Showa Chemical Co. (Tokyo, Japan). Diammonium phosphate, ammonia solution and nitric acid were obtained from Katayama Chemical Co. (Osaka, Japan). Sodium hydroxide was from Riedel-de Haën (Seelze, Germany). Copper standard solution (1000 mg/L) was bought from Merck (Darmstadt, Germany). All chemicals were used as received without further purification.

2.2. Synthesis of PGA-AP Nanoparticles

The PGA-AP nanoparticles were synthesized by coprecipitation of calcium nitrate and diammonium phosphate in the presence of γ-PGA, as reported by Boanini et al., with slight modification [21]. Briefly, 0.05 g of γ-PGA was dissolved in 50 g of deionized water and the pH of solution was adjusted to 10 with ammonia solution. Aqueous solutions of calcium nitrate and diammonium phosphate were separately prepared in concentrations of 1.08 and 0.65 M, respectively; in each was added ammonia solution to adjust pH to 10. Calcium nitrate and diammonium phosphate solutions were dropped simultaneously into the γ-PGA solution according to Ca/P molar ratio of 1.67 under magnetic stirring, and ammonia solution was added continuously to maintain the pH at 10. After dropping, the mixture was transferred to and sealed in a glass bottle, heated to 90 °C for 24 h and then cooled to room temperature. The precipitate was collected by centrifugation at 10,000 rpm for 10 min and washed three times with deionized water. Finally, the PGA-AP nanoparticles were dried at 60 °C for 24 h. The theoretical weight ratios of γ-PGA to AP were 1:20 (G1H20), 1:40 (G1H40) and 1:60 (G1H60).

2.3. Characterizations

The functional groups of PGA-AP were identified by a Bio-Rad FTS-40 spectrophotometer (Hercules, CA, USA) using KBr discs. A total of 64 scans within the range of 4000–500 cm^{-1} at a resolution of 2 cm^{-1} were collected and averaged for each sample.

The actual weight fraction of γ-PGA in the PGA-AP nanoparticles was roughly estimated by TGA on a TA 2050 (TA Instruments, New Castle, DE, USA). An amount of 5–10 mg of sample was heated from room temperature to 100 °C, maintained at 100 °C for 5 min and then heated to 650 °C with a heating rate of 10 °C/min. The weight fraction of γ-PGA in the nanoparticles were calculated as: $(W_2/W_1) \times 100\%$, where W_1 and W_2 represent the weight losses of γ-PGA and PGA-AP, respectively, in the 300–650 °C range [12].

The crystalline phase of PGA-AP was examined by a Rigaku MiniflexII X-ray diffractometer (Tokyo, Japan) equipped with Cu Kα radiation at 30 kV and 15 mA. Data were collected from 20° to 60° (2θ) at a scanning speed of 1°/min.

The calcium to phosphorus ratio of PGA-AP was measured by an EDS system connected to the field-emission scanning electron microscopy (JEOL JSM-6701F, Tokyo, Japan).

The particle size of PGA-AP nanoparticles was conducted by DLS (Brookhaven Instruments Co., 90Plus particle size analyzer, Holtsville, NY, USA) with deionized water as the dispersion medium.

2.4. Adsorption Experiments

2.4.1. Procedure

The adsorption of copper ions by PGA-AP nanoparticles was performed using the batch method. An amount of 0.025 g of PGA-AP nanoparticles was contacted with 50 mL of 100 ppm of copper solutions in a shaking bath at 100 rpm. The conditions affecting copper ions adsorption onto PGA-AP nanoparticles were studied by varying pH (4, 5 and 6), temperature (30, 45 and 60 °C) and contact time (1, 3, 5, 10, 30, 60, 180 and 720 min). The pH of the solution was adjusted with nitric acid and sodium hydroxide. After adsorption experiment, the suspension was centrifuged and the supernatant was taken to determine the residual concentration of copper ions by a flame atomic absorption spectrophotometer (model AA-400, Perkin Elmer, Waltham, MA, USA). A calibration curve was obtained by measuring different concentrations of the standard copper solutions (2, 3, 4, 5 and 6 ppm) at pH values of 4, 5 and 6, which were prepared by dilutions of the stock solution (1000 mg/L) with deionized water. The amount of copper ions adsorbed by PGA-AP nanoparticles at time t (q_t (mg/g)) was calculated from the following mass balance equation:

$$q_t = \frac{(C_0 - C_t)V}{m} \quad (1)$$

where C_0 and C_t (mg/L) are the concentrations of copper ions in solutions initially and at time t, respectively, V (L) is the volume of copper solution, and m (g) is the mass of PGA-AP nanoparticles (adsorbent). When t is equal to the equilibrium time, the amount of copper ions adsorbed by PGA-AP nanoparticles at equilibrium (q_e) can be calculated using the above equation (i.e., $C_t = C_e$, $q_t = q_e$).

2.4.2. Adsorption Kinetics

To understand the mechanism and kinetics of copper ions adsorption onto PGA-AP nanoparticles, the experimental data were fitted with two most common adsorption kinetic models, pseudo-first-order and pseudo-second-order model [22]. The deviation of the model from experimental data was evaluated by coefficient of determination (R^2).

The pseudo-first-order model assumes that the diffusion is the rate-limiting step of the adsorption process. The rate of adsorption is proportional to the number of unoccupied sites. It can be expressed as follows:

$$\frac{dq_t}{dt} = k_1(q_e - q_t) \quad (2)$$

The linear form is as follows:

$$\ln(q_e - q_t) = \ln q_e - k_1 t \quad (3)$$

where k_1 (1/min) is pseudo-first-order rate constant. The values of k_1 and q_e can be determined from the linear plot of $\ln(q_e - q_t)$ versus t.

The pseudo-second-order model assumes that the chemical adsorption is the rate-limiting step. The rate of adsorption is proportional to the square of the number of unoccupied sites. It can be presented as follows:

$$\frac{dq_t}{dt} = k_2(q_e - q_t)^2 \quad (4)$$

The linear form is given as:

$$\frac{t}{q_t} = \frac{1}{k_2 q_e^2} + \frac{t}{q_e} \quad (5)$$

where k_2 (g/(mg min)) is pseudo-second-order rate constant. The values of k_2 and q_e can be determined from the linear plot of t/q_t versus t.

2.4.3. Adsorption Isotherms

The adsorption isotherm describes the relation between the amounts of metal ion adsorbed onto adsorbent surface and the concentration of the metal ion remaining in the solution at a particular temperature when the adsorption process reaches equilibrium conditions. Various amounts of G1H20 nanoparticles (0.025, 0.035, 0.045, 0.055, 0.065 and 0.075 g) were added to 50 mL of 100 ppm of copper solutions at pH of 6 and 60 °C. The mixture was agitated in a shaking bath at 100 rpm for 720 min. The adsorption data were fitted with two commonly used isotherm models, Langmuir and Freundlich, to understand the adsorption behavior of copper ions onto PGA-AP nanoparticles.

The Langmuir isotherm model is based on monolayer adsorption onto a homogeneous adsorbent surface without any interactions between adsorbed molecules [23]. The Langmuir equation is given by:

$$q_e = \frac{q_m K_L C_e}{1 + K_L C_e} \quad (6)$$

The linear form is as follows:

$$\frac{C_e}{q_e} = \frac{1}{K_L q_m} + \frac{C_e}{q_m} \quad (7)$$

where q_m (mg/g) corresponds to the maximum amount of copper ions adsorbed per gram of adsorbent to form a complete monolayer on the surface. K_L (L/mg) is the Langmuir equilibrium constant related to the bonding-energy of the adsorbate to the adsorbent. The constants q_m and K_L can be determined from the slope and intercept of the linear plot between C_e/q_e and C_e.

The important characteristic of the Langmuir isotherm is the dimensionless separation factor (R_L), which confirms the favorability of the adsorption process and is expressed as follows:

$$R_L = \frac{1}{1 + K_L C_0} \quad (8)$$

where C_0 (mg/L) corresponds to the highest initial copper ion concentration in the solution.

The Freundlich isothermal model indicates the heterogeneity of the adsorbent surface and describes multilayer adsorption with an energetic nonuniform distribution [24]. The adsorption capacity is related to the concentration of copper ions at equilibrium and can be expressed as:

$$q_e = K_F C_e^{1/n} \quad (9)$$

The linear form is as follows:

$$\ln q_e = \ln K_F + \frac{1}{n} \ln C_e \quad (10)$$

where K_F [(mg/g)/(mg/L)$^{-1/n}$] and $1/n$ are the Freundlich constants related to the capacity and intensity of the adsorption, respectively. The constants K_F and $1/n$ can be determined from the intercept and slope of the linear plot between lnq_e and lnC_e.

3. Results and Discussion

3.1. PGA-AP Characteristics

The nucleation and growth of three PGA-AP nanoparticles in the presence of γ-PGA was performed by varying the theoretical weight ratios of γ-PGA to AP. The chemical composition and crystal structure of PGA-AP were characterized by FTIR, EDS, TGA and XRD analyses.

The FTIR spectrum of γ-PGA exhibited a strong and broad band around 3400 cm^{-1} (Figure 1), which could be attributed to both N–H and O–H stretching vibrations of amide groups and absorbed water, respectively [25]. The band around 2935 cm^{-1} belonged to C–H stretching vibration of alkyl chains. The N–H bending of amide II and stretching vibration of carboxylate salt group (COO^-) appeared at around 1589 and 1635 cm^{-1}, respectively [26]. The absorption band due to C=O stretching (amide I) was overlapped by that of COO^- [27]. In comparison of the FTIR spectra of PGA-AP and γ-PGA, PGA-AP exhibited additional strong and sharp bands at 564, 603, 634, 962, 1031 and 1095 cm^{-1} corresponding to stretching and bending vibrations of phosphate groups [28]. A sharp absorption band at 3570 cm^{-1} was due to hydroxyl ions (OH^-) stretching vibration. The weak absorption bands at 874, 1421 and 1455 cm^{-1} attributable to CO_3^{2-} ions, revealing that carbonate groups were incorporated into the apatite structure by substituting B-site of phosphate groups during synthesis [29,30]. The characteristic bands of γ-PGA were also shown in all the PGA-AP nanoparticles, indicating that γ-PGA was immobilized on the nanoparticles. Moreover, the relative intensities of the absorption bands at 2935, 1589 and 1635 cm^{-1} decreased with decreasing the γ-PGA content, indicating that less amount of γ-PGA was immobilized on the G1H60.

TGA was performed to quantitatively calculate the actual weight fraction of γ-PGA in the nanoparticles. Figure 2 shows TGA curves of γ-PGA and PGA-AP nanoparticles. A considerable amount of weight loss (35%) from 300 to 400°C was noticed for γ-PGA. The smaller weight loss (<6%) observed below 250 °C was attributed to water desorption because of the hydrophilic nature of γ-PGA. All PGA-AP exhibited a similar thermal behavior. The major weight loss occurred between 300 and 400 °C due to the thermal decomposition of γ-PGA present in the particles, which increased with increasing the γ-PGA content. The relative amounts of γ-PGA incorporation into G1H20, G1H40 and G1H60 were found to be about 6.0, 3.6 and 2.2 wt%, respectively.

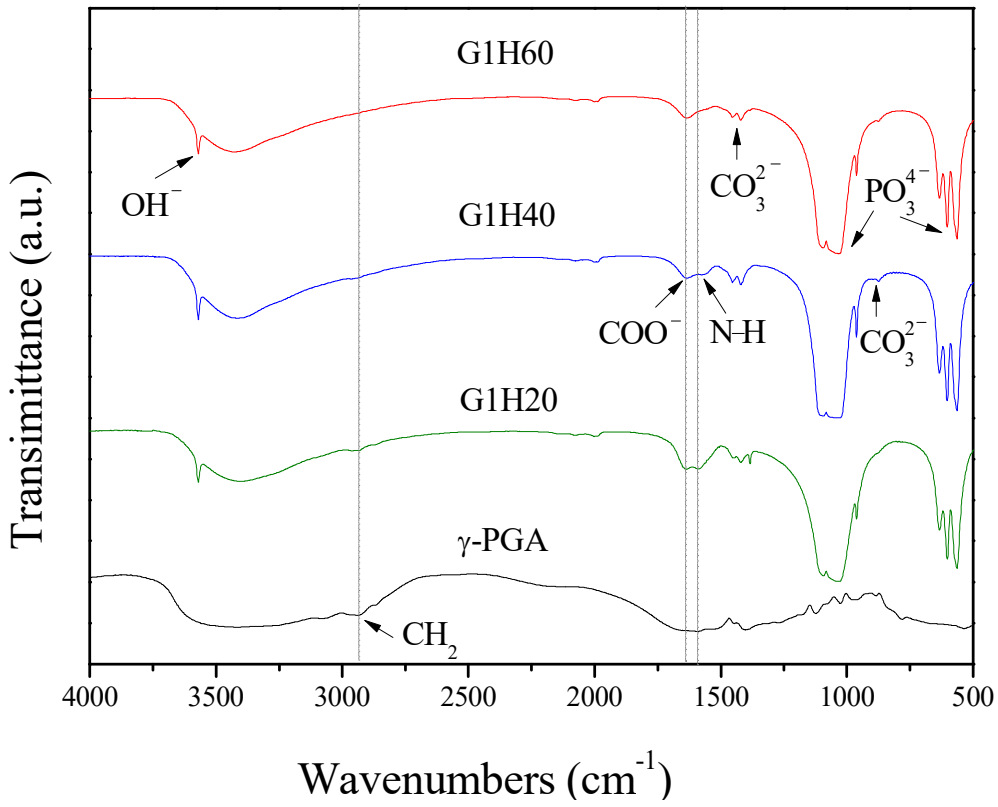

Figure 1. FTIR absorption spectra of poly-γ-glutamate (γ-PGA) and poly-γ-glutamate/apatite (PGA-AP) nanoparticles.

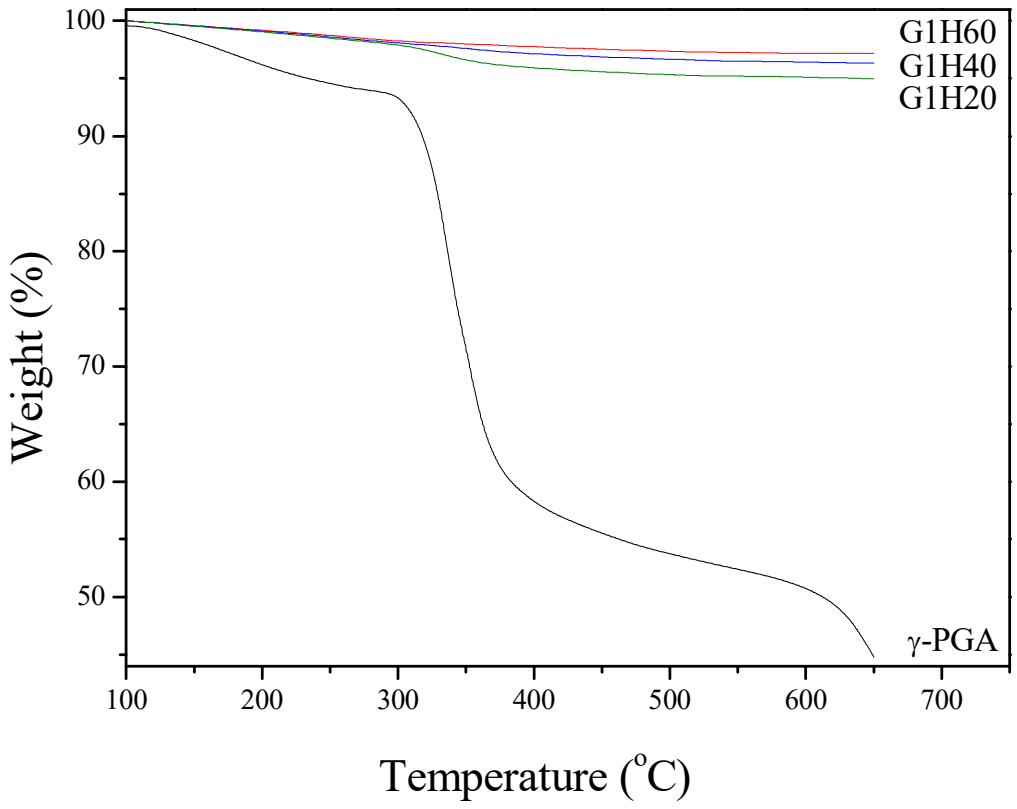

Figure 2. Thermal gravimetric analysis (TGA) curves of γ-PGA and PGA-AP nanoparticles.

XRD analysis was performed to identify the crystal phase of the synthesized precipitates. The XRD patterns of PGA-AP nanoparticles are illustrated in Figure 3. PGA-AP exhibited characteristic crystalline peaks at 2θ = 25.9°, 28.9°, 31.8°, 32.9°, 34.1°, 39.8°, 46.8°, 49.5° and 53.3° corresponding to (002), (210), (211), (112), (300), (310), (222), (321) and (004) crystallographic planes, respectively, which are the major reflections of hydroxyapatite crystals [19]. Therefore, the crystallographic data indicated the formation of hydroxyapatite crystals in the presence of γ-PGA. EDS analysis showed that the Ca/P atomic ratios of G1H20, G1H40 and G1H60 nanoparticles were 1.62, 1.58 and 1.76, respectively, which were close to the stoichiometric value for hydroxyapatite (1.67).

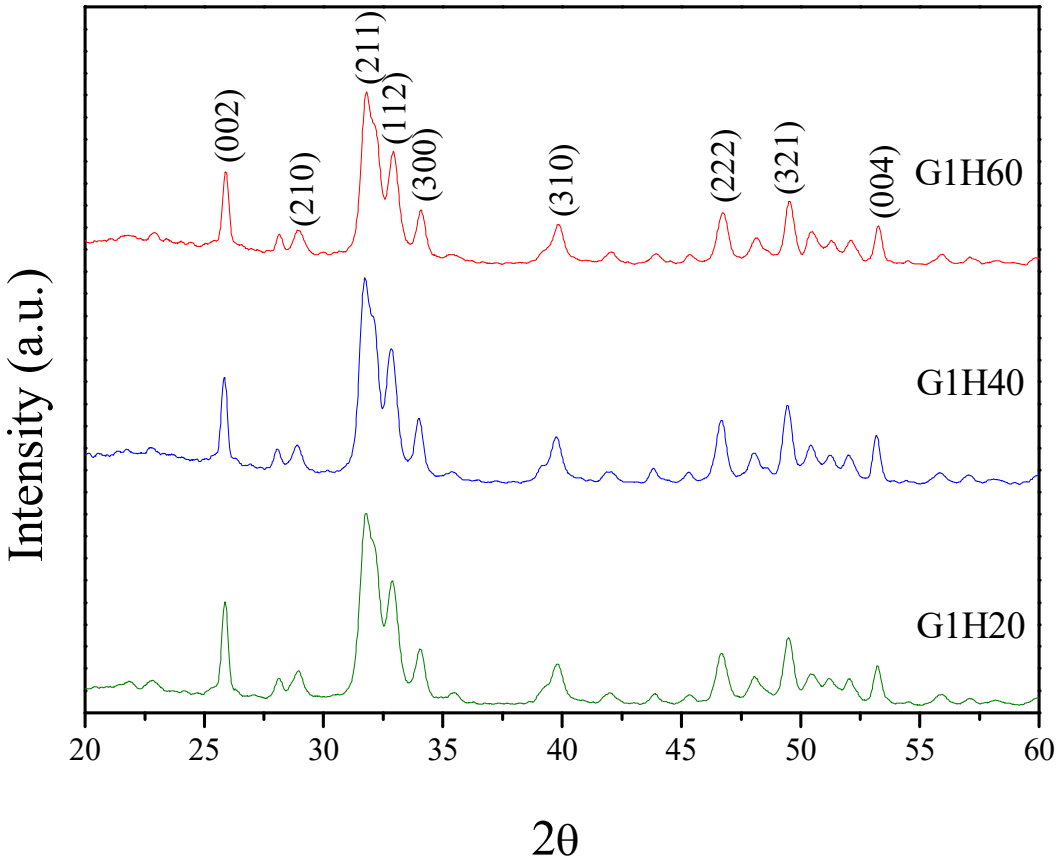

Figure 3. Powder X-ray diffraction (XRD) patterns of PGA-AP nanoparticles.

The particle sizes of G1H20, G1H40 and G1H60 measured by DLS were 79.7 ± 1.6, 88.5 ± 0.8 and 92.8 ± 2.3 nm, respectively, indicating they increased significantly with decreasing the γ-PGA content ($P < 0.05$).

3.2. Adsorption Study

The adsorption experiments were carried out to investigate the influence of different parameters, such as contact time, solution pH and temperature, on the adsorption of Cu(II) in a batch system. Figure 4 presents the adsorption capacity of Cu(II) onto PGA-AP nanoparticles with different weight ratios of γ-PGA to AP at a pH of 6 and 30 °C. The rapid adsorption was observed in the first 10 min. After that, a slight decrease was occurred until equilibrium was reached at around 60 min. Several previous studies also showed that heavy metal ions can be rapidly adsorbed by hydroxyapatites [31]. Moreover, the adsorption experiments demonstrated that the equilibrium adsorption capacity, q_e (mg/g), of Cu(II) onto PGA-AP nanoparticles was increased by increasing the γ-PGA content. The surface charges of hydroxyapatite particles is positive in acid solutions due to positively charged $\equiv CaOH_2^+$ and neutral ≡P–OH species on the surface [32].

Therefore, Cu(II) adsorption onto hydroxyapatite is related to other mechanisms. The main mechanisms of Cu(II) adsorption onto hydroxyapatite include ion exchange with Ca^{2+} of the hydroxyapatite, surface complexation with the P–OH groups of the hydroxyapatite, and partial dissolution of hydroxyapatite followed by the precipitation of a Cu-containing hydroxyapatite [33]. On the other hand, γ-PGA possesses abundant negatively charged carboxylates (pKa = 4.25) [34]. Moreover, the nitrogen atom of the amide group of γ-PGA can also complex with Cu(II) [17]. Therefore, the modification of hydroxyapatite with γ-PGA can provide additional active sites for Cu(II) adsorption. More carboxylate groups were available on the surface of the nanoparticles when the γ-PGA content increased. As expected, the q_e was increased from 54.99 mg/g for G1H60 to 63.29 mg/g for G1H20 (Figure 4). Similar results have been found by other investigators. Yang et al. reported that the adsorption capacity of the hydroxyapatite nanoparticles for Cu(II) was significantly enhanced through modification with humic acid, mainly because of the introduction of phenol and carboxylic groups on the surface of the nanoparticles [11]. Bachoua et al. found that the Pb(II) adsorption capacity was improved due to grafting of aspartic acid and glutamic acid onto hydroxyapatite [12]. Moreover, the higher adsorption capacity of G1H20 could be also attributed to its smaller particle size with increased surface area, which provided more adsorption sites for the removal of Cu(II). In the following experiments, the effect of temperatures and pH values on the adsorption of Cu(II) by G1H20 nanoparticles was investigated.

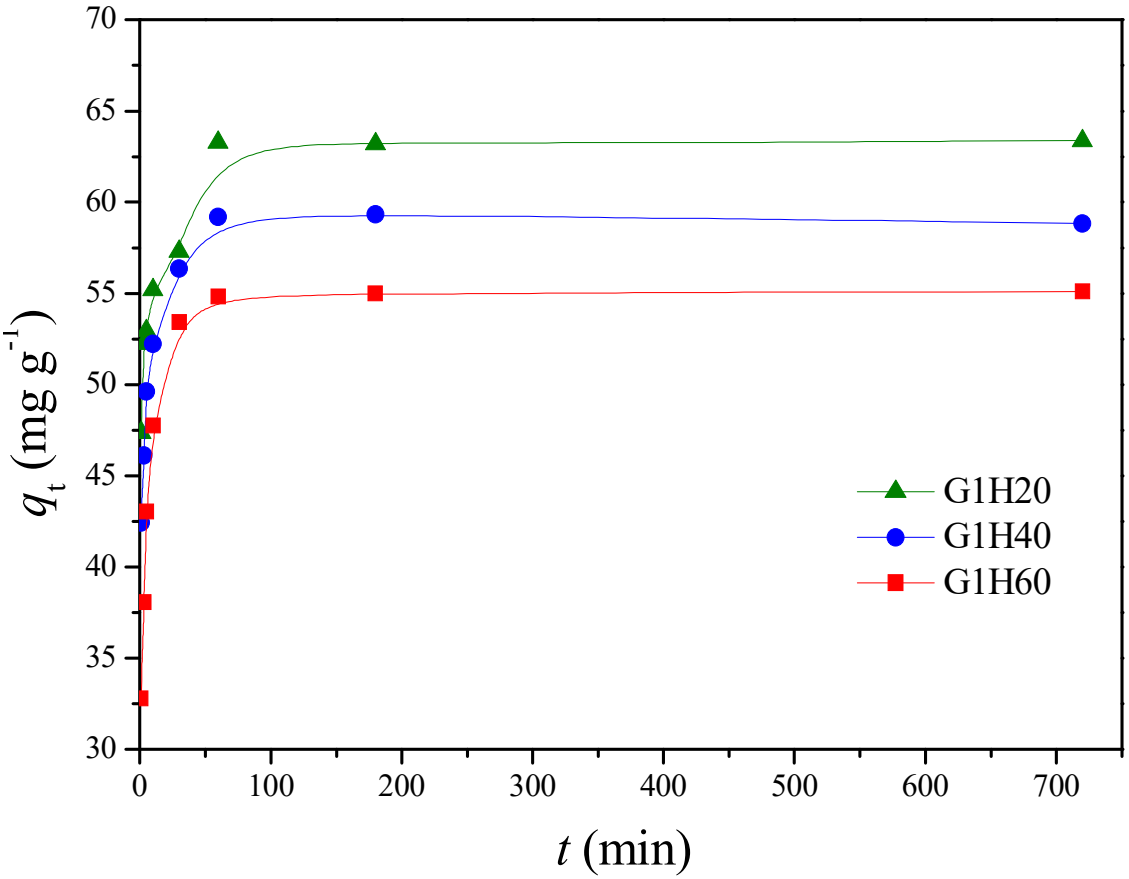

Figure 4. Comparison of Cu(II) adsorption onto PGA-AP nanoparticles with different weight ratios of γ-PGA to AP at a pH of 6 and 30 °C.

The effect of temperature on Cu(II) adsorption by G1H20 nanoparticles was evaluated over the range from 30 to 60 °C at a pH of 6 and 100 ppm of initial Cu(II) concentration. Figure 5 demonstrates that a rapid adsorption of Cu(II) by G1H20 was occurred within the first 10 min of contact time, followed by a gradual increase until reaching an equilibrium

value. Moreover, it was observed that increasing temperature had a positive effect on the adsorption capacity of G1H20 nanoparticles. The q_e was increased from 63.29 to 74.80 mg/g as the temperature rose from 30 to 60 °C, indicating that adsorption removal of Cu(II) by PGA-AP nanoparticles favored a high temperature. Similar results have been observed by other investigators [35].

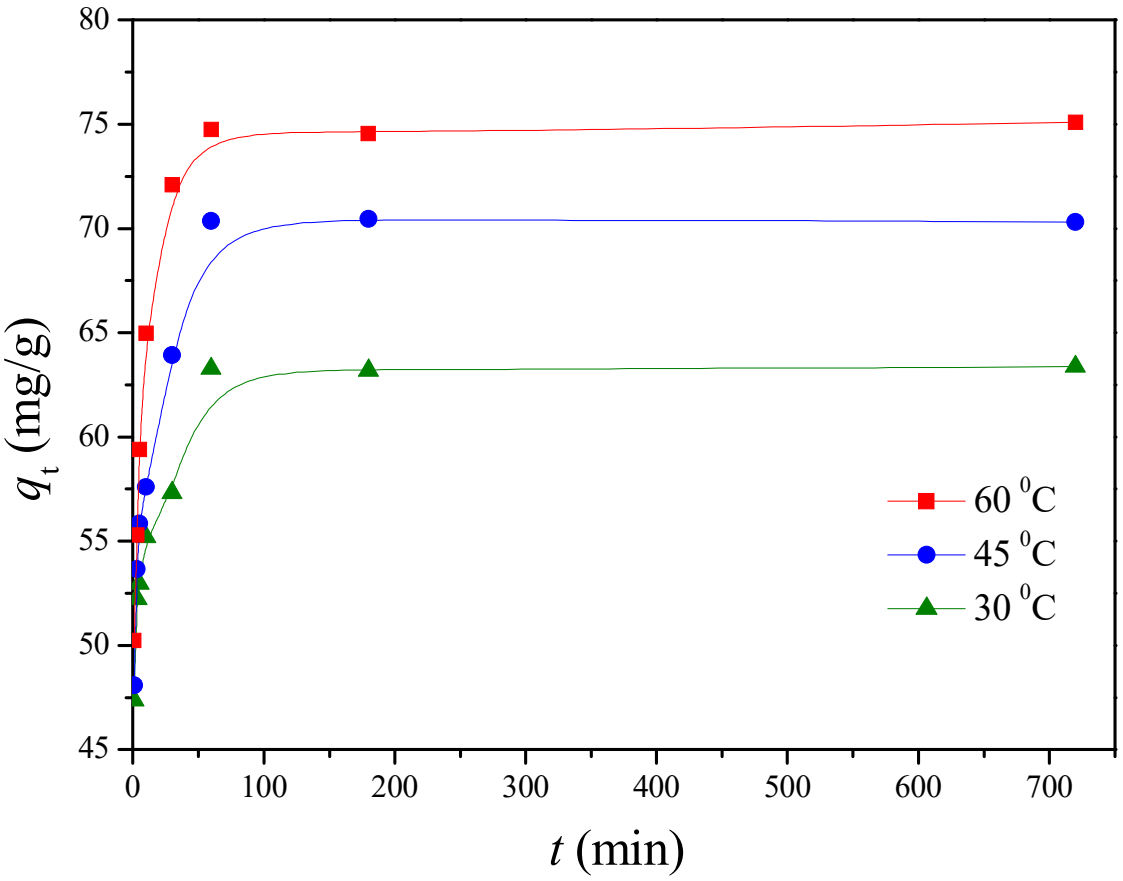

Figure 5. Effect of temperature on the adsorption of Cu(II) onto G1H20 nanoparticles at a pH of 6.

The pH of the solution is an important parameter in the removal of heavy metals from wastewater and aqueous solutions because it affects not only the degree of ionization of metal ions in solution but also the charge of adsorbents [36]. The chemical forms of Cu(II) present in aqueous solution, such as Cu(II), $Cu(OH)^+$, $Cu_2(OH)_2{}^{2+}$, $Cu(OH)_2$, $Cu(OH)_3{}^-$, and $Cu(OH)_4{}^{2-}$, are known to depend on the pH of the aqueous solution [37]. Cu(II) is the dominant species at pH below 6.5 [38]. Solid $Cu(OH)_2$ (Ksp = 2.2 × 10^{-20}) starts to precipitate above pH of 6.5 [39,40]. Thus, the adsorption capability at pH beyond 6 was not studied. The influence of pH on Cu(II) adsorption by G1H20 nanoparticles was studied by varying the pH from 4 to 6 at 60 °C and 100 ppm of initial Cu(II) concentration. As shown in Figure 6, the adsorption rate of Cu(II) was rapid during the first 10 min and reached equilibrium after 60 min. The q_e was increased from 52.98 to 74.80 mg/g as solution pH increased from 4 to 6. The carboxylate groups of the G1H20 nanoparticles were partially protonated to generate carboxylic acid groups at lower pH, which results in competition between Cu(II) and hydrogen ions for the same adsorption sites [41]. Yang et al. found that the adsorbed amount of Cu(II) was increased with increasing the solution pH from 2.5 to 6.5 [11]. Siao et al. revealed that the maximum binding amounts of Pb(II) and Cd(II) by γ-PGA were occurred in the pH range of 5 to 7 [42]. They also reported that an appreciable adsorption of Hg(II) by γ-PGA was observed at pH beyond 3 and reached a maximum at a pH of 6 [15]. Additionally, the surface of hydroxyapatite particles is net positively charged

at low pH conditions, which is less favorable in complexing metal cations on the adsorbent surface [43,44]. Therefore, the G1H20 nanoparticles can adsorb more Cu(II) at a pH of 6.

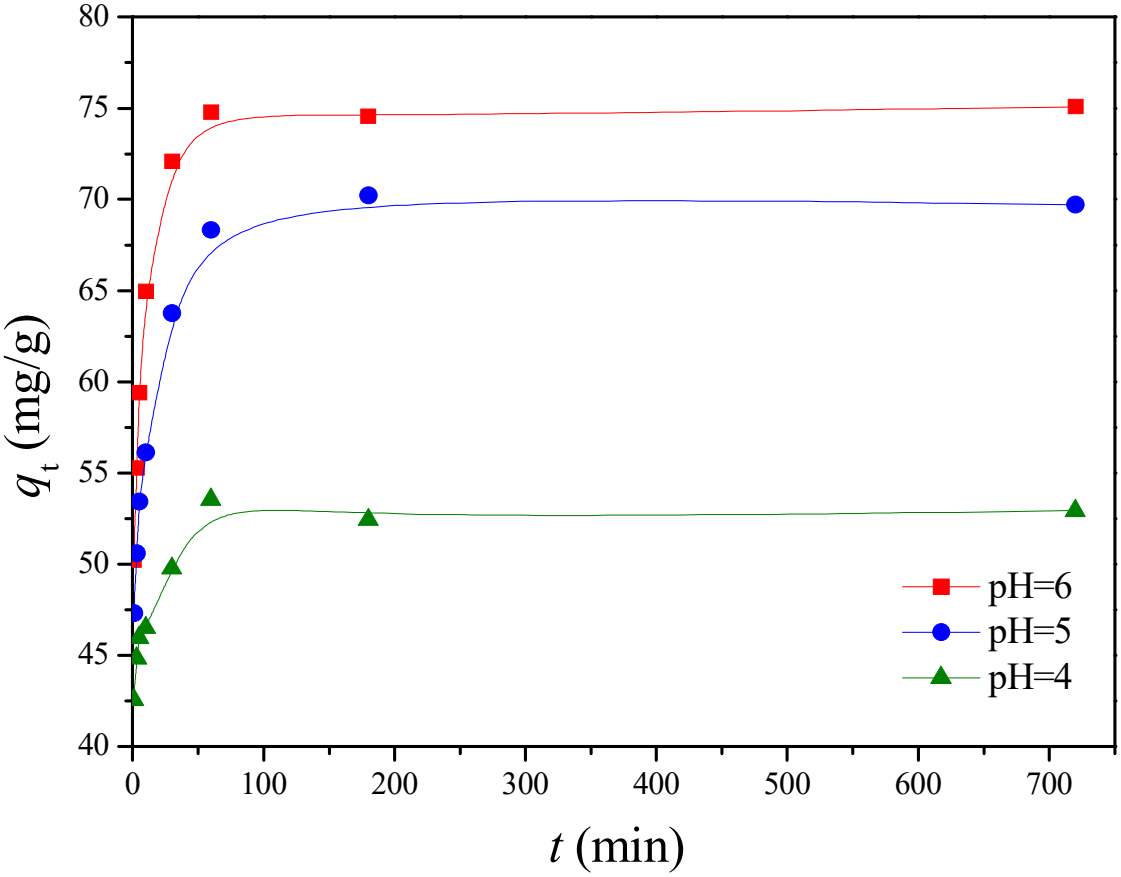

Figure 6. Effect of pH on the adsorption of Cu(II) onto G1H20 nanoparticles at 60 °C.

3.2.1. Adsorption Kinetics

Two well-known kinetic models, a pseudo-first order equation of Lagergren based on solid capacity and a pseudo-second order equation based on solid phase adsorption, were applied to evaluate the mechanism of adsorption [43]. Figures 7–9 show the linear plots of pseudo-first-order and pseudo-second-order models for the adsorption of Cu(II) onto different PGA-AP nanoparticles at different temperatures and pH values, respectively. The adsorption kinetic constants and correlation coefficients (R^2) for both pseudo-first and pseudo-second-order kinetics are presented in Table 1. As shown in Table 1, The calculated q_e values from the pseudo-first-order kinetic model were much different from the experimental ones, indicating that it was not appropriate to describe the adsorption process. It is clear from R^2 values that the adsorption process of Cu(II) onto PGA-AP nanoparticles obeyed the pseudo-second-order kinetic model better than the first-order kinetic model. Most of previous studies reported that the adsorption kinetics of Cu(II) by the hydroxyapatite-containing composites followed the pseudo-second-order kinetic model [45]. The R^2 values for the pseudo-second-order kinetic model were nearly equal to 1 (>0.997), and the calculated q_e values agreed very well with the experimental ones. These results suggest that the rate-limiting step in the adsorption process may be chemical adsorption involving valence forces via electrons sharing or exchange between the PGA-AP nanoparticles and Cu(II) [46,47].

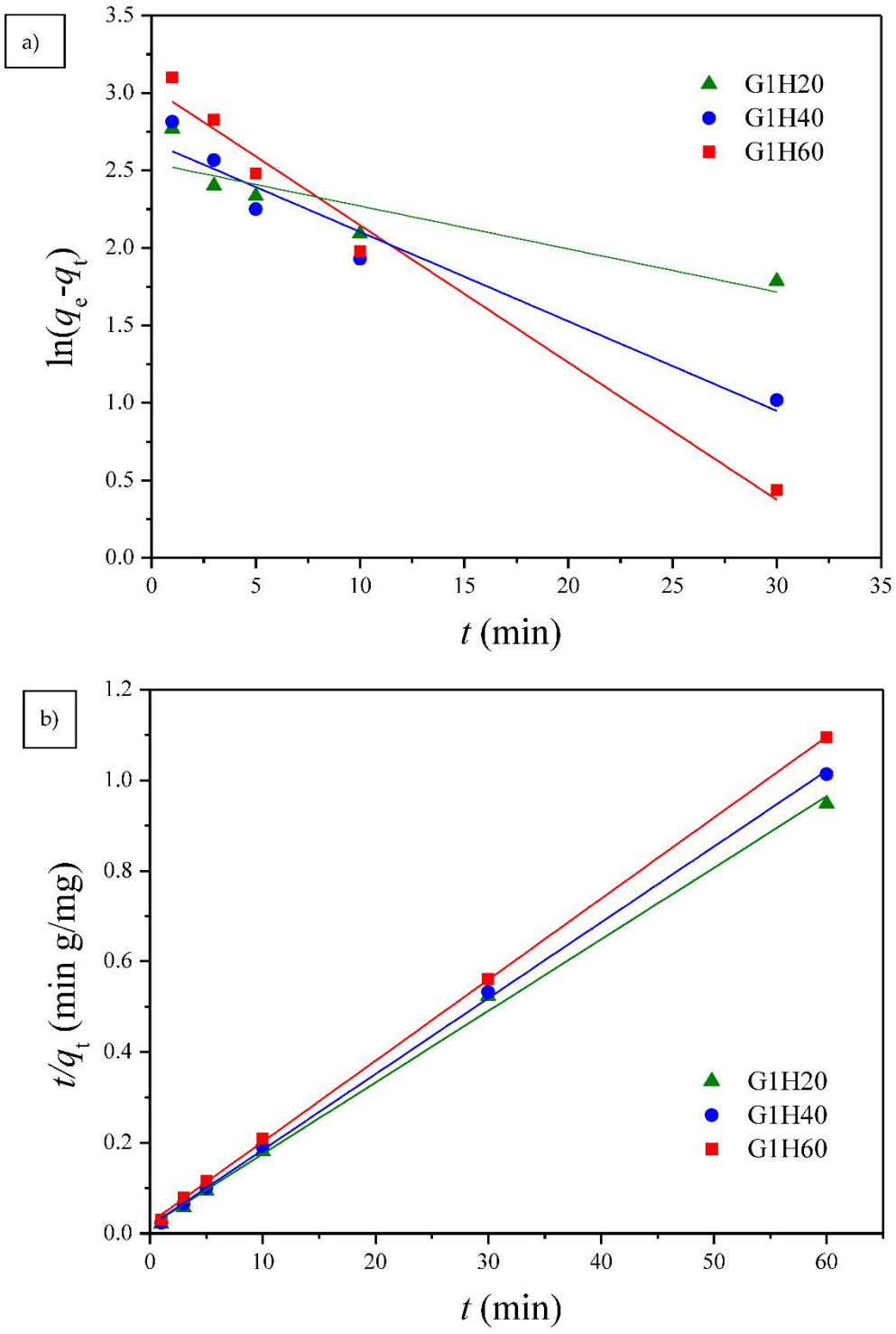

Figure 7. The (**a**) pseudo-first order and (**b**) pseudo-second order kinetic models for Cu(II) adsorption onto PGA-AP nanoparticles with different weight ratios of γ-PGA to AP at a pH of 6 and 30 °C.

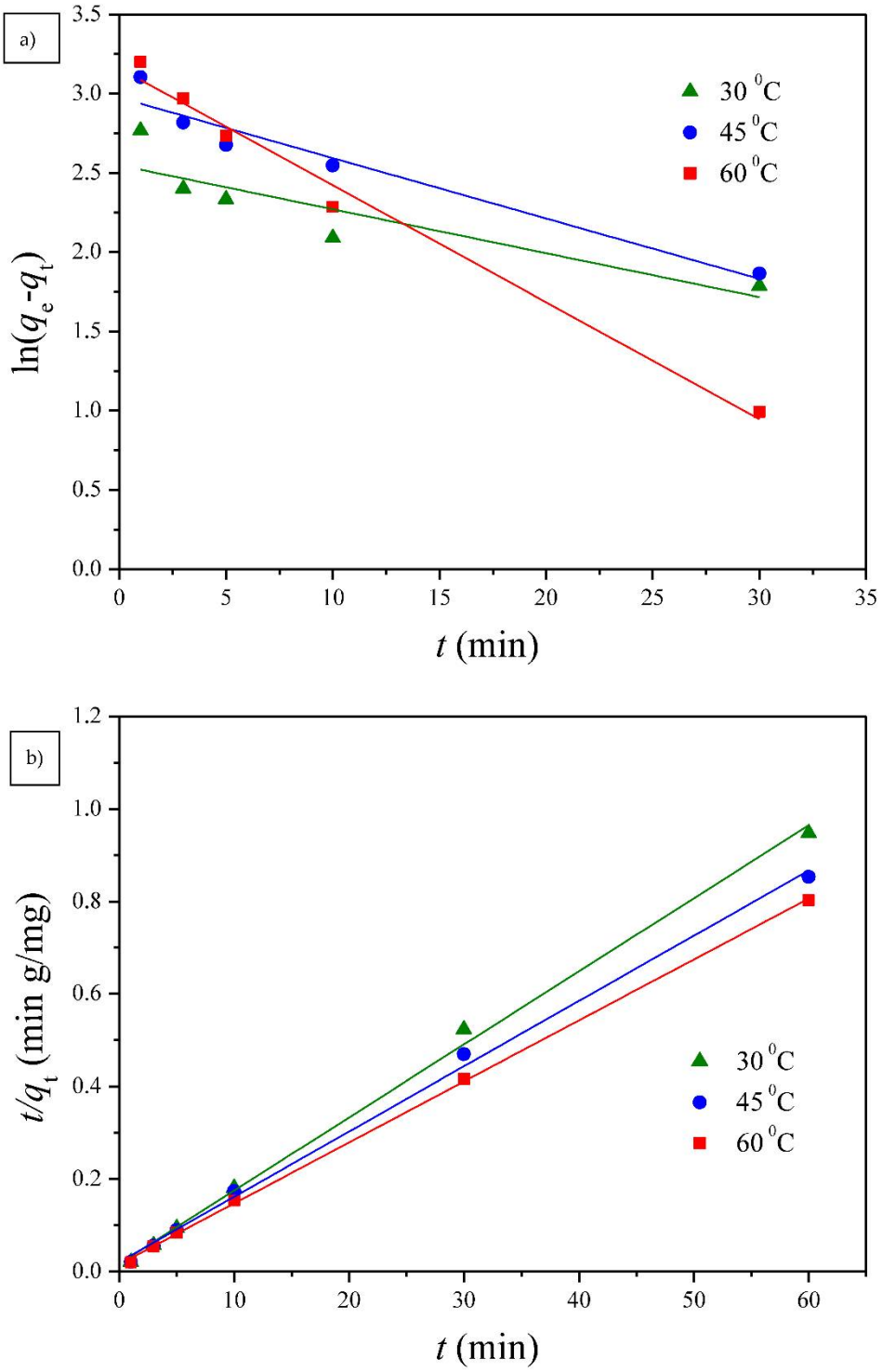

Figure 8. The (**a**) pseudo-first order and (**b**) pseudo-second order kinetic models for Cu(II) adsorption onto G1H20 nanoparticles at a pH of 6 and different temperatures.

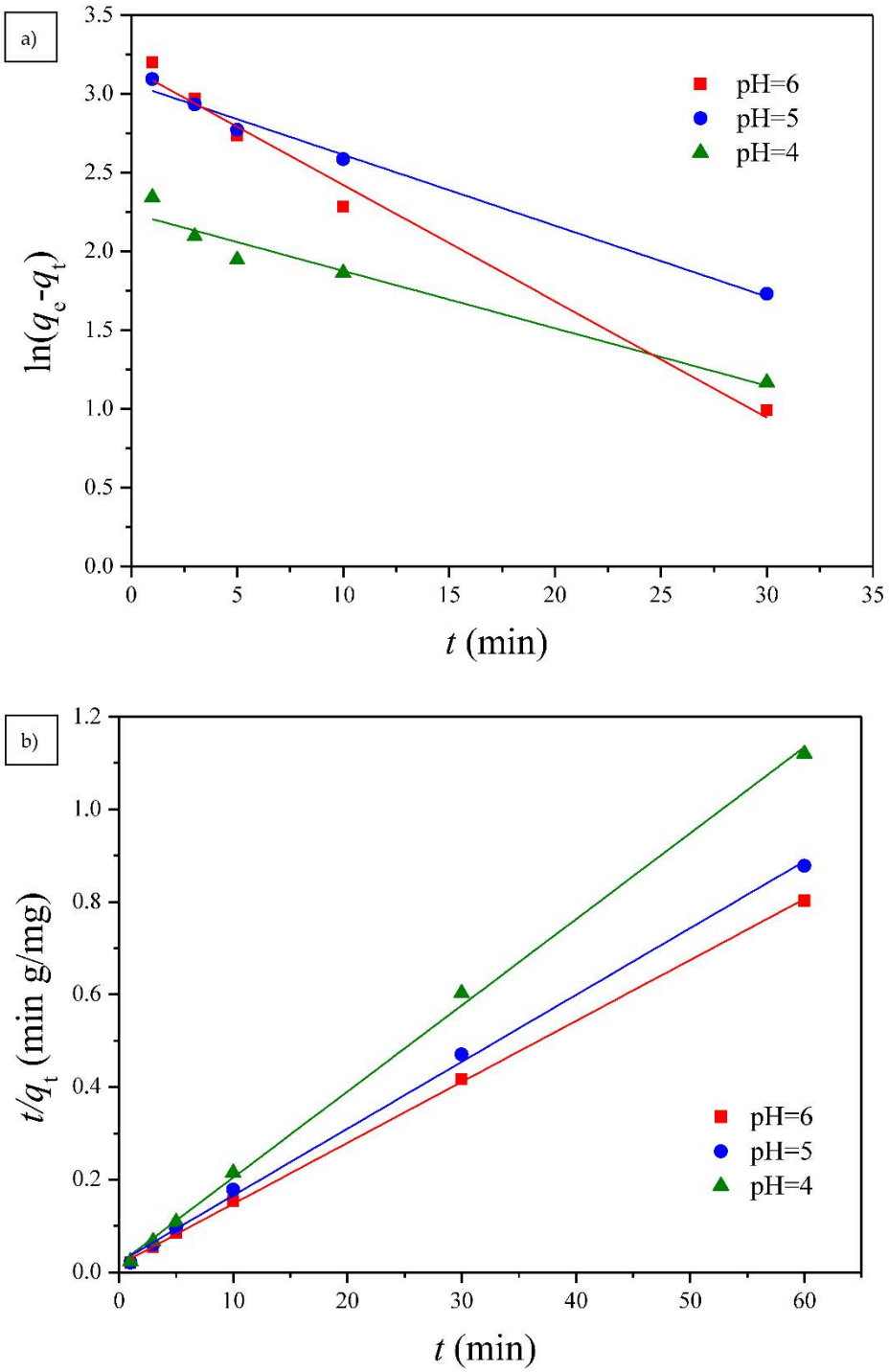

Figure 9. The (**a**) pseudo-first order and (**b**) pseudo-second order kinetic models for Cu(II) adsorption onto G1H20 nanoparticles at 60 °C and different pH values.

Table 1. Pseudo-first-order and pseudo-second-order kinetic model constants for Cu(II) adsorption onto PGA-AP nanoparticles.

Materials	Temperature (°C)	pH	q_e, exp (mg/g)	Pseudo-First-Order Model Constants			Pseudo-Second-Order Model Constants		
				q_e, cal (mg/g)	k_1 (1/min)	R^2	q_e, cal (mg/g)	k_2 (g/(mg min))	R^2
G1H20	30	6	63.29	12.79	2.78×10^{-2}	0.7303	63.37	1.42×10^{-2}	0.9971
G1H40	30	6	59.13	14.62	5.78×10^{-2}	0.9348	59.77	1.63×10^{-2}	0.9993
G1H60	30	6	54.99	20.77	8.86×10^{-2}	0.9783	55.96	1.35×10^{-2}	0.9997
G1H20	45	6	70.37	19.60	3.81×10^{-2}	0.9298	70.92	9.52×10^{-3}	0.9971
G1H20	60	4	52.98	9.42	3.65×10^{-2}	0.9416	53.73	1.90×10^{-2}	0.9983
G1H20	60	5	69.41	21.45	4.51×10^{-2}	0.9866	69.20	9.93×10^{-3}	0.9983
G1H20	60	6	74.80	23.62	7.39×10^{-2}	0.9834	75.93	1.09×10^{-2}	0.9995

3.2.2. Adsorption Isotherms

Langmuir and Freundlich isotherm models were used to investigate the adsorption equilibrium of the PGA-AP nanoparticles for Cu(II) adsorption. The absorption data were fitted to the linear forms of the Langmuir and Freundlich isotherms for Cu(II) adsorption onto G1H20 nanoparticles at a pH of 6 and 60 °C and are illustrated in Figure 10. The obtained isotherm model constants and R^2 values are summarized in Table 2. The maximum adsorption capacity (q_m) calculated from Langmuir equation (78.99 mg/g) was close to the experimental value (74.80 mg/g). The Langmuir equilibrium constant (K_L) was 2.23×10^{-1} L/mg. The dimensionless separation factor (R_L) was 0.0429, which was in the range of 0 to 1, indicating favorable adsorption of Cu(II) onto PGA-AP nanoparticles. The Freundlich adsorption capacity (K_F) was determined to be 50.41. The adsorption intensity ($1/n$) was 0.0904, which was less than 1, indicating that Cu(II) was easily adsorbed by PGA-AP nanoparticles. The R^2 value of the Langmuir isotherm (0.9978) is higher than the obtained value from the Freundlich isotherm (0.9066), suggesting that the adsorption of Cu(II) form a monolayer onto the surface of PGA-AP nanoparticles. The result is consistent with other previous studies [5,45,48].

Table 2. Langmuir and Freundlich isotherm constants for Cu(II) adsorption onto G1H20 nanoparticles at a pH of 6 and 60 °C.

Langmuir Isotherm Model				Freundlich Isotherm Model		
q_m (mg/g)	K_L (L/mg)	R_L	R^2	K_F [(mg/g)/(mg/L)$^{-1/n}$]	1/n	R^2
78.99	2.23×10^{-1}	4.29×10^{-2}	0.9978	50.41	9.04×10^{-2}	0.9066

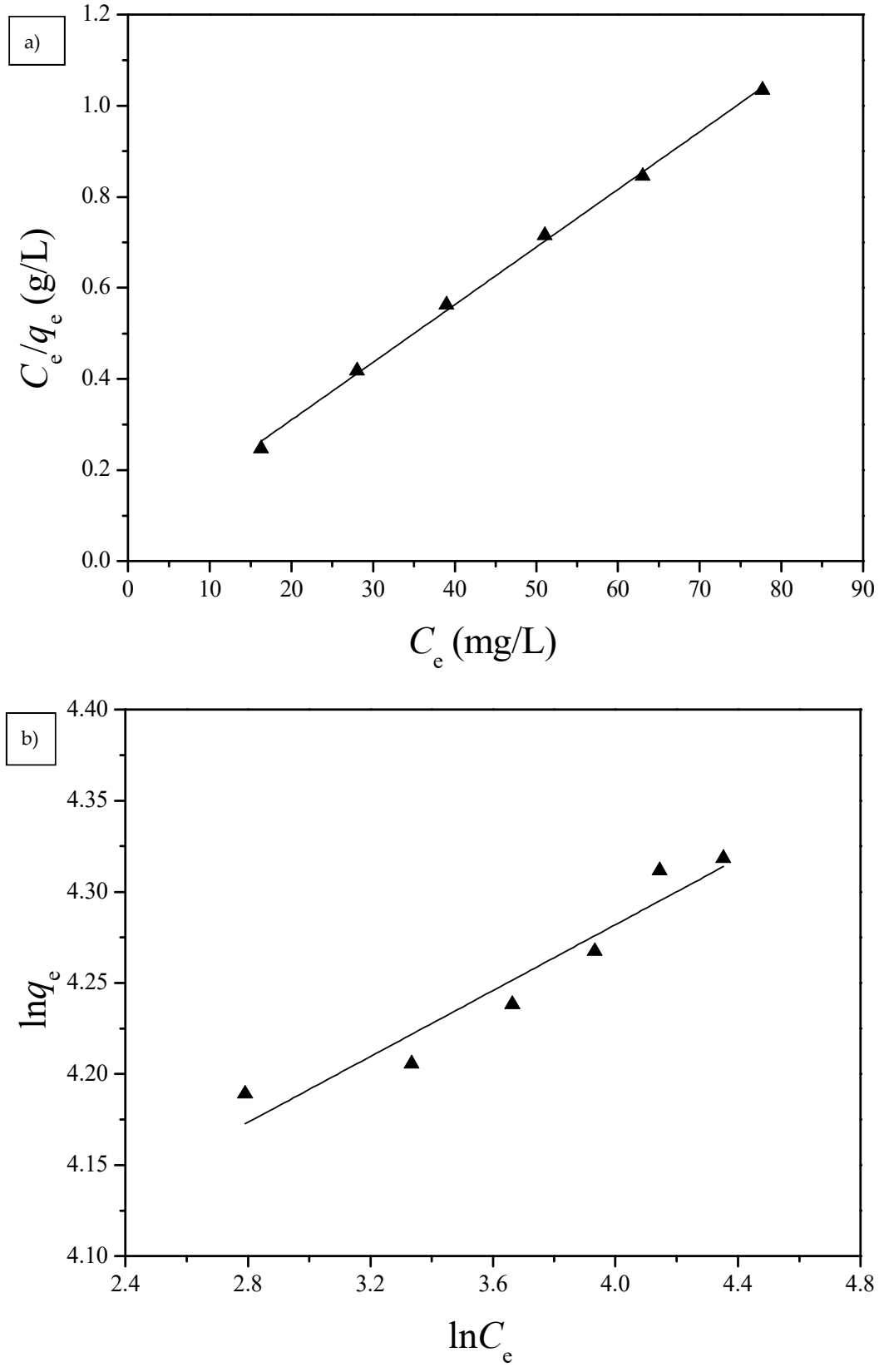

Figure 10. (**a**) Langmuir and (**b**) Freundlich isotherms for the adsorption of Cu(II) by G1H20 nanoparticles at a pH of 6 and 60 °C.

4. Conclusions

PGA-AP nanoparticles with 2.2 to 6.0 wt% of γ-PGA were synthesized as adsorbents for removing Cu(II) from aqueous solution. The composition and structure of PGA-AP were confirmed by FTIR, TGA, XRD and EDS. The particle size of PGA-AP nanoparticles decreased significantly with the increase of γ-PGA content. It was also found that the Cu(II) adsorption amount of PGA-AP nanoparticles was increased with increasing the immobilized amount of γ-PGA. The equilibrium adsorption capacity of about 74.80 mg/g was achieved at pH of 6 and 60 °C after 60 min of contact time. The adsorption kinetics and isotherms investigations demonstrated that the Cu(II) adsorption by PGA-AP nanoparticles followed well the pseudo-second-order kinetics and the Langmuir isotherm equation, respectively. It suggests that the Cu(II) adsorption process was mainly chemical adsorption and monolayer adsorption.

Author Contributions: Conceptualization, investigation, and writing, K.-Y.C.; methodology and formal analysis, W.-Y.Z. All authors have read and agreed to the published version of the manuscript.

Funding: We like to thank the Ministry of Science and Technology of the Republic of China, Taiwan (contract No. MOST 103-2221-E-224-011) for financially supporting this research.

Institutional Review Board Statement: Not applicable.

Informed Consent Statement: Not applicable.

Data Availability Statement: Data is contained within the article.

Conflicts of Interest: The authors declare no conflict of interest.

References

1. Mustafa, S.K.; AlSharif, M.A. Copper (Cu) an essential redox-active transition metal in living system: A review article. *Am. J. Anal. Chem.* **2018**, *9*, 15–26. [CrossRef]
2. Nose, Y.; Rees, E.M.; Thiele, D.J. Structure of the Ctr1 copper trans 'PORE'ter reveals novel architecture. *Trends Biochem. Sci.* **2006**, *31*, 604–607. [CrossRef] [PubMed]
3. Burakov, A.E.; Galunin, E.V.; Burakova, I.V.; Kucherova, A.E.; Agarwal, S.; Tkachev, A.G.; Gupta, V.K. Adsorption of heavy metals on conventional and nanostructured materials for wastewater treatment purposes: A review. *Ecotoxicol. Environ. Saf.* **2018**, *148*, 702–712. [CrossRef]
4. Krstić, V.; Urošević, T.; Pešovski, B. A review on adsorbents for treatment of water and wastewaters containing copper ion. *Chem. Eng. Sci.* **2018**, *192*, 273–287. [CrossRef]
5. Fernane, F.; Boudia, S.; Aiouache, F. Removal Cu(II) and Ni(II) by natural and synthetic hydroxyapatites: A comparative study. *Desalin. Water Treat.* **2014**, *52*, 2856–2862. [CrossRef]
6. Ferri, M.; Campisi, S.; Scavini, M.; Evangelisti, C.; Carniti, P.; Gervasini, A. In-Depth study of the mechanism of heavy metal trapping on the surface of hydroxyapatite. *Appl. Surf. Sci.* **2019**, *475*, 397–409. [CrossRef]
7. Campisi, S.; Castellano, C.; Gervasini, A. Tailoring the structural and morphological properties of hydroxyapatite materials to enhance the capture efficiency towards copper(II) and lead(II) ions. *New J. Chem.* **2018**, *42*, 4520–4530. [CrossRef]
8. Wadhawan, S.; Jain, A.; Nayyar, J.; Mehta, S.K. Role of nanomaterials as adsorbents in heavy metal ion removal from waste water: A review. *J. Water Process Eng.* **2020**, *33*, 101038. [CrossRef]
9. Okada, M.; Matsumoto, T. Synthesis and modification of apatite nanoparticles for use in dental and medical applications. *Jpn. Dent. Sci. Rev.* **2015**, *51*, 85–95. [CrossRef]
10. Smičiklas, I.D.; Lazić, V.M.; Živković, L.S.; Porobić, S.J.; Ahrenkiel, S.P.; Nedeljković, J.M. Sorption of divalent heavy metal ions onto functionalized biogenic hydroxyapatite with caffeic acid and 3,4-dihydroxybenzoic acid. *J. Environ. Sci. Health A* **2015**, *54*, 899–905. [CrossRef] [PubMed]
11. Yang, L.; Wei, Z.; Zhong, W.; Cui, J.; Wei, W. Modifying hydroxyapatite nanoparticles with humic acid for highly efficient removal of Cu(II) from aqueous solution. *Colloids Surf. A Physicochem. Eng. Asp.* **2016**, *490*, 9–21. [CrossRef]
12. Bachoua, H.; Renaudin, G.; Badraoui, B.; Leroux, F.; Debbabi, M.; Nedelec, J.M. Preparation and characterization of functionalized hybrid hydroxyapatite from phosphorite and its potential application to Pb^{2+} remediation. *J. Sol. Gel Sci. Technol.* **2016**, *78*, 621–631. [CrossRef]
13. Halmschlag, B.; Hoffmann, K.; Hanke, R.; Putri, S.P.; Fukusaki, E.; Büchs, J.; Blank, L.M. Comparison of isomerase and Weimberg pathway for γ-PGA production from xylose by engineered *Bacillus subtilis*. *Front. Bioeng Biotechnol.* **2020**, *7*, 476. [CrossRef]
14. Shih, L.; Van, Y.T. The production of poly-(γ-glutamic acid) from microorganisms and its various applications. *Bioresour. Technol.* **2001**, *79*, 207–225. [CrossRef]

15. Inbaraj, B.S.; Wang, J.S.; Lu, J.F.; Siao, F.Y.; Chen, B.H. Adsorption of toxic mercury(II) by an extracellular biopolymer poly(γ-glutamic acid). *Bioresour. Technol.* **2009**, *100*, 200–207. [CrossRef] [PubMed]
16. Bodnár, M.; Hajdu, I.; Rőthi, E.; Harmati, N.; Csikós, Z.; Hartmann, J.F.; Balogh, C.; Kelemen, B.; Tamas, J.; Borbély, J. Biopolymer-based nanosystem for ferric ion removal from water. *Sep. Purif. Technol.* **2013**, *112*, 26–33. [CrossRef]
17. Karmaker, S.; Saha, T.K.; Sakurai, H. Investigation of a CuII-poly(γ-glutamic acid) complex in aqueous solution and its insulin-mimetic activity. *Macromol. Biosci.* **2007**, *7*, 456–466. [CrossRef] [PubMed]
18. Ben Moussa, S.; Mehri, A.; Gruselle, M.; Beaunier, P.; Costentin, G.; Badraoui, B. Combined effect of magnesium and amino glutamic acid on the structure of hydroxyapatite prepared by hydrothermal method. *Mater. Chem. Phys.* **2018**, *212*, 21–29. [CrossRef]
19. Wang, Z.; Xu, Z.; Zhao, W.; Sahai, N. A potential mechanism for amino acid-controlled crystal growth of hydroxyapatite. *J. Mater. Chem. B* **2015**, *3*, 9157–9167. [CrossRef]
20. Park, S.B.; Hasegawa, U.; Van Der Vlies, A.J.; Sung, M.H.; Uyama, H. Preparation of poly(γ-glutamic acid)/hydroxyapatite monolith via biomineralization for bone tissue engineering. *J. Biomater. Sci. Polym. Ed.* **2014**, *25*, 1875–1890. [CrossRef] [PubMed]
21. Boanini, E.; Torricelli, P.; Gazzano, M.; Giardino, R.; Bigi, A. Nanocomposites of hydroxyapatite with aspartic acid and glutamic acid and their interaction with osteoblast-like cells. *Biomaterials* **2006**, *27*, 4428–4433. [CrossRef] [PubMed]
22. Ho, Y.S. Review of second-order models for adsorption systems. *J. Hazard. Mater.* **2006**, *136*, 681–689. [CrossRef] [PubMed]
23. Langmuir, I. The adsorption of gases on plane surfaces of glass, mica and platinum. *J. Am. Chem. Soc.* **1918**, *40*, 1361–1403. [CrossRef]
24. Freundlich, H. Über die adsorption in lösungen. *Z. Phys. Chem.* **1907**, *57*, 385–470. [CrossRef]
25. Inbaraj, B.S.; Kao, T.H.; Tsai, T.Y.; Chiu, C.P.; Kumar, R.; Chen, B.H. The synthesis and characterization of poly(γ-glutamic acid)-coated magnetite nanoparticles and their effects on antibacterial activity and cytotoxicity. *Nanotechnology* **2011**, *22*, 075101. [CrossRef]
26. Wu, H.D.; Ji, D.Y.; Chang, W.J.; Yang, J.C.; Lee, S.Y. Chitosan-Based polyelectrolyte complex scaffolds with antibacterial properties for treating dental bone defects. *Mater. Sci. Eng. C Mater. Biol. Appl.* **2012**, *32*, 207–214. [CrossRef]
27. Yu, S.H.; Wu, S.J.; Tang, D.W.; Ho, Y.C.; Mi, F.L.; Kuo, T.H.; Sung, H.W. Stimuli-Responsive materials prepared from carboxymethyl chitosan and poly(γ-glutamic acid) for protein delivery. *Carbohydr. Polym.* **2012**, *87*, 531–536. [CrossRef]
28. Zhang, G.; Chen, J.; Yang, S.; Yu, Q.; Wang, Z.; Zhang, Q. Preparation of amino-acid-regulated hydroxyapatite particles by hydrothermal method. *Mater. Lett.* **2011**, *65*, 572–574. [CrossRef]
29. Qi, M.L.; Qi, J.; Xiao, G.Y.; Zhang, K.Y.; Lu, C.Y.; Lu, Y.P. One-Step hydrothermal synthesis of carbonated hydroxyapatite porous microspheres with a large and uniform size regulated by L-glutamic acid. *CrystEngComm* **2016**, *18*, 5876–5884. [CrossRef]
30. Yang, Y.; Wu, Q.; Wang, M.; Long, J.; Mao, Z.; Chen, X. Hydrothermal synthesis of hydroxyapatite with different morphologies: Influence of supersaturation of the reaction system. *Cryst. Growth Des.* **2014**, *14*, 4864–4871. [CrossRef]
31. Hashimoto, Y.; Sato, T. Removal of aqueous lead by poorly-crystalline hydroxyapatites. *Chemosphere* **2007**, *69*, 1775–1782. [CrossRef] [PubMed]
32. Pan, X.; Wang, J.; Zhang, D. Sorption of cobalt to bone char: Kinetics, competitive sorption and mechanism. *Desalination* **2009**, *249*, 609–614. [CrossRef]
33. Chen, J.H.; Wang, Y.J.; Zhou, D.M.; Cui, Y.X.; Wang, S.Q.; Chen, Y.C. Adsorption and desorption of Cu(II), Zn(II), Pb(II), and Cd(II) on the soils amended with nanoscale hydroxyapatite. *Environ. Prog. Sustain. Energy* **2010**, *29*, 233–241. [CrossRef]
34. Wyss, A.; Von Stockar, U.; Marison, I.W. Production and characterization of liquid-core capsules made from cross-linked acrylamide copolymers for biotechnological applications. *Biotechnol. Bioeng.* **2004**, *86*, 563–572. [CrossRef]
35. Elkady, M.F.; Mahmoud, M.M.; Abd-El-Rahman, H.M. Kinetic approach for cadmium sorption using microwave synthesized nano-hydroxyapatite. *J. Non. Cryst. Solids* **2011**, *357*, 1118–1129. [CrossRef]
36. Shen, H.; Pan, S.; Zhang, Y.; Huang, X.; Gong, H. A new insight on the adsorption mechanism of amino-functionalized nano-Fe_3O_4 magnetic polymers in Cu(II), Cr(VI) co-existing water system. *Chem. Eng. J.* **2012**, *183*, 180–191. [CrossRef]
37. Sheng, G.; Li, J.; Shao, D.; Hu, J.; Chen, C.; Chen, Y.; Wang, X. Adsorption of copper(II) on multiwalled carbon nanotubes in the absence and presence of humic or fulvic acids. *J. Hazard. Mater.* **2010**, *178*, 333–340. [CrossRef]
38. Rosskopfová, O.; Galamboš, M.; Ometáková, J.; Čaplovičová, M.; Rajec, P. Study of sorption processes of copper on synthetic hydroxyapatite. *J. Radioanal. Nucl. Chem.* **2012**, *293*, 641–647. [CrossRef]
39. Zhao, G.; Zhang, H.; Fan, Q.; Ren, X.; Li, J.; Chen, Y.; Wang, X. Sorption of copper(II) onto super-adsorbent of bentonite-polyacrylamide composites. *J. Hazard. Mater.* **2010**, *173*, 661–668. [CrossRef]
40. Liu, Y.; Chen, M.; Yongmei, H. Study on the adsorption of Cu(II) by EDTA functionalized Fe_3O_4 magnetic nano-particles. *Chem. Eng. J.* **2013**, *218*, 46–54. [CrossRef]
41. Park, J.A.; Kang, J.K.; Lee, S.C.; Kim, S.B. Electrospun poly(acrylic acid)/poly(vinyl alcohol) nanofibrous adsorbents for Cu(II) removal from industrial plating wastewater. *RSC Adv.* **2017**, *7*, 18075–18084. [CrossRef]
42. Siao, F.Y.; Lu, J.F.; Wang, J.S.; Inbaraj, B.S.; Chen, B.H. In vitro binding of heavy metals by an edible biopolymer poly(γ-glutamic acid). *J. Agric. Food Chem.* **2009**, *57*, 777–784. [CrossRef]
43. Zhang, W.; Wang, F.; Wang, P.; Lin, L.; Zhao, Y.; Zou, P.; Zhao, M.; Chen, H.; Liu, Y.; Zhang, Y. Facile synthesis of hydroxyapatite/yeast biomass composites and their adsorption behaviors for lead(II). *J. Colloid Interface Sci.* **2016**, *477*, 181–190. [CrossRef] [PubMed]

44. Liao, D.; Zheng, W.; Li, X.; Yang, Q.; Yue, X.; Guo, L.; Zeng, G. Removal of lead(II) from aqueous solutions using carbonate hydroxyapatite extracted from eggshell waste. *J. Hazard. Mater.* **2010**, *177*, 126–130. [CrossRef]
45. Bazargan-Lari, R.; Zafarani, H.R.; Bahrololoom, M.E.; Nemati, A. Removal of Cu(II) ions from aqueous solutions by low-cost natural hydroxyapatite/chitosan composite: Equilibrium, kinetic and thermodynamic studies. *J. Taiwan Inst. Chem. Eng.* **2014**, *45*, 1642–1648. [CrossRef]
46. Lu, S.; Gibb, S.W. Copper removal from wastewater using spent-grain as biosorbent. *Bioresour. Technol.* **2008**, *99*, 1509–1517. [CrossRef]
47. Ho, Y.S.; McKay, G. The kinetics of sorption of divalent metal ions onto sphagnum moss peat. *Water Res.* **2000**, *34*, 735–742. [CrossRef]
48. El Hamidi, A.; Arsalane, S.; Halim, M. Kinetics and isotherm studies of copper removal by brushite calcium phosphate: Linear and non-linear regression comparison. *Eur. J. Chem.* **2012**, *9*, 1532–1542. [CrossRef]